Response to the reviewers for paper OE-D20-01516: *Evolution of Lift in a Pure Cruciform for Energy Harvesting*

We would like to express our gratitude to the anonymous reviewers for their time and insight. Below, we document the comments from the reviewers and our response to the comments. We indicate the changes in the original manuscript using the colour blue.

Answers to Reviewer 1

Comment R1.1

Why OpenFOAM is employed? If other software can be employed to solve the calculation?

Answer to R1.1

In our opinion, any CFD software can be employed by a proficient enough user as a means to gain important insight on a subject of study. A numerical study in the area of fluid mechanics, as in other disciplines, can be of differing levels of complexity. Some are meant to be instructional, and these deal with relatively idealised cases, especially in a classroom setting. However, in a post-graduate or industrial setting, we think it is in the interest of the researcher(s) that the tool chosen to execute the numerical study fulfill the following criteria.

1. The algorithm required to carry out the numerical work must be built into the software. Else, the software itself must be easily extensible to include the numerical routine required.

2. A high degree of automation must be possible on any aspect of the numerical work, be it meshing, running and control of the simulation, data collection and parameter variation.

3. Parallellisation is built in to the software.

4. A stable software code base.

5. The software allows real-time collaboration with multiple authors across a common platform, allowing each iteration of the project or parts of it to be version controlled.

6. Cost-effective.

OpenFOAM, which at the most fundamental level is a collection of C++ library, is easily modified and extended (point 1) using nothing more than a plain text editor, and then recompiled to include the required functionality. The use of extensible text editors such as VIM or Emacs greatly facilitates this process, and at zero cost.

Any aspect of the workflow using OpenFOAM can be automated (point 2) through the use of PyFOAM, a Python library that allows fine-grain control of virtually every aspect of the simulation. In addition to automating the grid independency study and parameter variation, PyFOAM can also be used to post-process data by exploiting the NumPy Python library. Furthermore, parallellisation is built into the OpenFOAM code (point 3), and the fact that the code is open source, facilitates the discovery and patching of bugs (point 4).

Usage of the OpenFOAM software involves including and modifying configuration files, written as plain text files. As such, one can easily leverage the pre-existing tools used by software engineers such as Git, enabling real-time collaboration (point 5) between project members and provide much-needed version control of the whole project. We would like to point out all the tools mentioned in the previous discussion are available for free, incurring zero extra cost on the team, which can be beneficial especially for new and emerging laboratories, where procurement of hardwares is of higher priority.

Comment R1.2

Mesh independence test is carried out using GCI method, but I think the reference can be updated. For example:[Applied Thermal Engineering. 2020;171:115090], [https://doi.org/10.1016/j.energy.2020.118690].

Answer to R1.2

Following the suggestion from the reviewer, we added the following sentence in the revised manuscript.

> A common method for checking the grid independency of quantities of interest in a numerical study is by demonstrating that one obtained similar results on all variants of the spatial discretisation (usually three grids), and then proceeding with the numerical study using the medium variant on the computational domain (see e.g., Ding et al. (2013), Ding et al. (2019), or Wang et al. (2020), who settled on the coarse variant of their spatial discretisation).

Comment R1.3

Some figures' resolution need to be adjusted.

Answer to R1.3

We re-exported the figures used in the revised manuscript directly into the PDF format instead

of the PNG format used previously, for better resolution as per the suggestion of the reviewer.

Comment R1.4

Boundary conditions need to be shown.

Answer to R1.4

In the revised manuscript, we included the boundary conditions in Table 1, and added the description of Table 1 as follows.

> Table 1 summarises the boundary conditions imposed on each of the boundary patches in the simulation domain (see Fig. 6). The symbols U, p, ν_T, and $\tilde{\nu}$ refer to the flow velocity, pressure, kinetic eddy viscosity and its mediating variable, respectively. At the inlet, the `fixedValue` for U is the freestream velocity U_∞ (m/s), while $U = 0\,\text{m/s}$ at the strip plate. The `fixedValue` for p at the outlet is $0\,\text{m}^2/\text{s}^2$, and the `fixedValue` for $\tilde{\nu}$ is $0\,\text{m}^2/\text{s}$ at the cylinder and strip plate patches.

Answers to Reviewer 2

Comment R2.1

It's suggested to define FIM in line 37 of page 3 (sub-section 2.1), even though it's easy to know that FIM means flow-induced motion.

Answer to R2.1

We have added the definition of FIM, which is flow-induced motion, in the revised manuscript following the suggestion by the reviewer.

Comment R2.2

Why chose the distance of $7.5D$ from front/back boundary to centre of cylinder (Fig 2)? And how did the boundary condition set in this study?

Answer to R2.2

We considered a few factors in determining the spanwise dimension of the simulation domain, and they fall in one of the following two categories. First, adherence to the physical manifestation of streamwise vortex shedding, as observed in experimental studies. Under this category, we note the minimum spanwise half-length of a system that required for the expression of streamwise vortex-induced vibration (SVIV) is between $2D$ to $3.2D$ (e.g., Shirakashi et al. (2001) and Koide et al. (2006)). Taking this into consideration, we doubled the length of the latter, obtaining $3.2D \times 2 = 6.4D$, and then applying a safety factor of approximately 1.2, or exactly 1.17875, arriving at a round number of $15D$ for the total spanwise length of the simulation domain, and $15D/2 = 7.5D$ as its half-length.

The second category involves evaluating the actual implementation of spanwise lengths in similar numerical studies of SVIV. Numerical studies of SVIV, or simply the numerical study of streamwise vortex shedding from a cruciform stucture are relatively few and far between. This is probably due to the irreducibility of the SVIV phenomenon to a two-dimensional (2D) problem, thus rendering it more computationally demanding than the numerical study of Karman vortices shedding and by extension, Karman vortex-induced vibration (KVIV). Here, we shall discuss the spanwise lengths implemented in the handful of numerical work on SVIV and how they influece our choice of spanwise length in the manuscript.

The earliest numerical work on SVIV from a cruciform system that we know of is the study by Deng et al. (2007). In the paper, the authors used a spanwise length of $12D$ and identified different vibration responses of the cruciform according to the spacing of the upstream and downstream cylinders. Fast forward about a decade and we find the study by Hemsuwan et al. (2018a), which

has an equivalent spanwise length of $13D$, in Hemsuwan et al. (2018c) with an equivalent spanwise length of $14.5D$ and in Hemsuwan et al. (2018b) with an equivalent length of $16D$. All of the studies mentioned deal with cruciform systems that elicit motion of the upstream cylinder resulting from the shedding of streamwise vortices. As such, it became apparent to us that our choice of domain spanwise length, $15D$, is well within the trend found in comparable literature, which lies between $12D$ and $16D$, providing further basis to our decision.

There is one case (Zhao and Lu, 2018) in which the authors implemented a spanwise length of $42D$ in their computational domain. This particular study, however, is limited to a fixed cruciform in which both of the cylinders forming the cruciform are fixed. In our opinion, by limiting their scope to a fixed cruciform, the authors of Zhao and Lu (2018) significantly eased their computational requirements - permitting them to implement a larger spanwise dimension compared to us, or the other studies we have discussed.

As for the boundary conditions, we refer the reviewer to our reply to comment 4 of reviewer 1.

Comment R2.3

It's suggested to presented or validated the time step (or nondimensionalised time step) of the simulation in this work.

Answer to R2.3

In this work, we used the Courant–Friedrichs–Lewy (CFL) number as the basis for our choice of time step implemented in the simulation. The CFL number is of course defined as

$$C = \frac{U\Delta t}{\Delta x}, \tag{1}$$

where C is the CFL number, U the flow velocity, Δt the time step and Δx the length a cell in the discretised domain, respectively. The time step Δt is chosen such that the condition $C < 1$ is always satisfied everywhere in the computational domain. Following the suggestion by the reviewer, we have added the following sentences in the revised manuscript.

> As for the temporal discretisation, we relied on a simple CFL number-based scheme (Hemsuwan et al., 2018a,c,b), in which the time step is chosen such the maximum CFL number C in the computational domain is always less than unity. The CFL number C, is defined in Eq. 21 as
>
> $$C = \frac{U\Delta t}{\Delta x}, \tag{21}$$
>
> where U, Δt and Δx represents the flow velocity, time step and characteristic length of cell, respectively.

Comment R2.4

In line 30 of page 15, why the sudden jump followed by a gradual drop and a gradual rise in y^*_{RMS} can be observed in this study but not in woks of Nguyen et al. (2012) nor Koide et al. (2013)? Any difference of parameters leads to the different results?

Answer to R2.4

A review of the literature on streamwise vortex shedding, with a particular focus on discussions about the degree of generated disturbance in the flow, or the level of flow turbulence, reveals three important takeaways.

1. The onset of streamwise vortex shedding brings with it an increased level of turbulence in the flow. This increases the uncertainty in the measurement of the root-mean-square value of normalised vibration amplitude y^*_{RMS} (Shirakashi et al., 1989; Zhao and Lu, 2018).

2. The level of turbulence generated in the flow following the onset of streamwise vortex shedding is higher when the cruciform is comprised of an upstream circular cylinder and downstream strip plate, in contrast to a cruciform made of two circular cylinders. This is evidenced by the broader distribution of cruciform downstream velocity fluctuation frequencies in the frequency domain (Kato et al., 2006, 2012), and also flow visualisations (Kato et al., 2012; Koide et al., 2017).

3. In a cruciform system whose constituents are an upstream circular cylinder and a downstream strip plate, systems whose plate width to cylinder diameter ratio is equal to unity, $W = w/D = 1$, generates a higher level of turbulence compared to cruciforms with $W < 1$ (Kato et al., 2012).

The turbulence intensity in our simulations is set to 5%, to recreate the ambient flow conditions our experimental setup is exposed to. This level of 5% is comparatively high, considering that the studies we used to benchmark our results operate in water tunnels with a turbulence level that is at 2.8% maximum (Nguyen et al., 2012; Koide et al., 2013). Add this to the fact that we are using a

1. circular cylinder-strip plate cruciform, and,

2. the $W = w/D$ for our strip plate is $W = 1$,

the level of turbulence in the flow, and the level of disturbance/noise resulting from it becomes an increasingly important factor in determining the evolution of the dominant flow structures, and

the resulting cylinder amplitude response. The jump-drop-rise pattern observed in the amplitude responses of both our experimental and numerical work is, in our opinion, the result of an interplay between the level of disturbance/noise due to increasingly turbulent flow conditions and the ability of the streamwise vortex to withstand said disturbance. As we have alluded to in the manuscript,

> " We, therefore, attribute this difference to the higher turbulence level set in our work. The turbulence level in the works of Nguyen et al. (2012), for example, was $< 2.8\%$ throughout their range of Reynolds number. Instead, the initial turbulence level in our setup, both experimental and numerical, is approximately double that value. Because of this, the turbulence amplification due to the onset of streamwise vortices (Zhao and Lu, 2018) - especially for a circular cylinder-strip plate cruciform (Koide et al., 2017) - is also higher compared to the experiments of Nguyen et al. (2012) and Koide et al. (2013). This higher compound turbulence warps the dominant vortical structure and introduces an increasing amount of intermittency to the lift signal, and by extension, to the displacement time history of the cylinder. "

In our opinion, the interplay between the level of disturbance in the flow and the streamwise vortices goes as follows.

- **Sudden jump:** At the onset of SVIV, the level of disturbance is still relatively small as the system has just barely entered the streamwise vortex shedding regime. This occurs at $U^* = 18.2$, where the vortical structures are the least deformed, and because of that, the net lift driving the vibration is higher compared to when the level of flow disturbance starts to grow.

- **Gradual drop:** As we increase U^*, the level of disturbance in the flow brought about by the rising turbulence increasingly warps the streamwise vortical structures, imparting a growing degree of intermittency on the lift and hence cylinder displacement signal ($20.5 \leq U^* \leq 22.7$). An increased intermittency in the cylinder displacement signal lowers its mean amplitude, which in this work is computed as y^*_{RMS}.

- **Gradual rise:** As we advance further into the SVIV regime ($U^* > 22.7$), the streamwise vortices becomes even more energised and increasingly resilient to ambient disturbance. This results in a less intermittent lift, the effect of which is imparted on the cylinder displacement signal, shown in Fig. 11(b) of the revised manuscript.

We acknowledge a lack of explanation on this matter in the original manuscript, and have therefore included the following sentences in the revised manuscript.

> An intermittent lift signal imposes the same trend on the $y^*(t)$ signal, reducing its overall mean amplitude, which we compute in this work as y^*_{RMS}.

and,

> We interpret this as the vortical structures becoming more energised and resilient against ambient excitation the further we advance into the SVIV regime.

Comment R2.5

The CFD over predict the frequency response and the value of St in low reduced velocity range (Fig 10), is this caused by the boundary condition or the size of computational domain?

Answer to R2.5

In the original manuscript, we explained the discrepancy highlighted by the reviewer as follows.

" The discrepancies found especially in Fig. 10b most probably stem from the same reasons explained by Nguyen et al. (2012). The lowest y^*_{RMS} recorded in our simulation within $6.8 \leq U^* \leq 13.6$ was in the order of 10^{-5} m (10 microns). A numerical study has no problem recording vibration of this order as the precision of the numerical solution is only limited by the processor architecture. Experimental work, however, requires not only the sensitivity but also the isolation from the background noise that forces the cylinder to vibrate close to the natural frequency of the system f_n (Nguyen et al., 2012), which consequently overpowers this minimal amplitude vibration. Once streamwise vortices form, however, their shedding and cylinder vibration synchronises close to f_n, thus locking the normalised vibration frequency back to $f^* \approx 1$. "

Recall that the frequency overshoot occurs at within a range of U^* where the vibration amplitude of the cylinder is especially small. In fact, this region of especially small vibration amplitude - in the order of 10 microns in our simulation - has been reported by Nguyen et al. (2012) and Nguyen et al. (2010) as the region where selective resonance takes place (see, e.g., §4.3 of Nguyen et al. (2010) and §4.3 of Nguyen et al. (2012)). When said selective resonance takes place, the randomly appearing external excitation causes the frequency spectra of the cylinder displacement to register a frequency close to the natural frequency of the system f_n - in other words, $f^* \approx 1$ - as the dominant frequency, overpowering the actual frequency at which the cylinder vibrates. In our humble understanding of their work, Nguyen et al. (2010) and Nguyen et al. (2012) simply excluded the data points that results from the selective resonance - all of which are close to f_n - from their frequency response plot. We provide the original quote from §4.3 of Nguyen et al. (2012) below.

" It is noted that when the oscillation amplitude is small in air flow, the spectrum of displacement, S_z, has a peak at f_n, in addition to f_v, due to the selective resonance which commonly occurs for a low-damped system exerted by alternating force having broadly distributing spectrum as shown in Fig. 4. In Fig. 7, and in the following figures in this paper, such data for f_z are not plotted. "

We decided to adopt a different approach and reported our experimental results as-is, including those affected by the selective resonance. This is why our experimental measurement of f^* returns a value close to 1 within $6.8 \leq U^* \leq 13.6$. However, numerical studies are immune from the random external excitations that experimental investigations are subject to, unless they are explicitly defined in the numerical setup. Therefore, the overshot values of f^* are in our humble opinion the limit to which f^* will approach as random, external perturbations on the flow approaches zero.

Acknowledging the inadequacy of our explanation in the original manuscript, we added the following sentence in the revised version.

The values of f^* between $6.8 \leq U^* \leq 13.6$ can therefore be considered as the limit f^* in that region, which is appoached as the random background forcing present in experimental works tend to zero.

Comment R2.6

It's interested that the fluctuation exists in Fig 11(a) when $U^* = 22.7$, how this exist and how the value of y^*_{RMS} and f^* calculated for this case (The values can be found in Fig 10)?

Answer to R2.6

The fluctuations that exist at $U^* = 22.7$ are the direct result of the vortex structure - turbulence level interplay mechanism explained in the answer for question 4.

We compute the root-mean-square value of a given quantity using the formula in Eq. 2.

$$y^*_{\mathrm{RMS}} = \frac{1}{N} \sqrt{\sum_{i=1}^{i=N} (y^*_i)^2}. \tag{2}$$

Here, N is the total number of data points, and y^*, the normalised cylinder displacement value. Equation 2 is used to compute the values of y^*_{RMS} at all U^*, including at $U^* = 22.7$.

We compute the values for f^* by performing the ensemble empirical mode decomposition (EEMD) on the normalised cylinder displacement signal y^*. Then, we take the component with the largest root-mean-square amplitude and compute its Hilbert transform, giving us the instantaneous frequency, a quantity that is a function of time. Finally, we compute the mean of that instantaneous

frequency signal, giving us the characteristic frequency of y^*, designated as f. Normalising f with f_n gives us f^*. The values of f^* at all U^* are computed using this method, including that at $U^* = 22.7$. The values of f^* can also be computed via fast Fourier transform (FFT), which yields similar results.

The reason we opted for the method above to compute f^* is because we are able to obtain the instantaneous frequency signal of y^* during the process of computing phase lag between y^* and f^*, which greatly steamlines our simulation post-processing, instead of running the results separately through FFT for the sole purpose of estimating f^*. To highlight this point, we included the following sentence in our revised manuscript.

> Here, f^* is computed as the mean instantaneous frequency of the dominant component of y^*, which we obtain in the course of calculating the phase lag between y^* and lift. The procedure employed to decompose the y^* signal and obtain the instantaneous frequency is elaborated in §5.1.

Comment R2.7

Looks like that the values still going to decline in Fig 12(a). It means that the vibration here still doesn't stable?

Answer to R2.7

The y^* and Cl signals presented in Fig. 12(a) are the results at $U^* = 4.5$, and at $U^* = 4.5$, the cylinder vibration is in the initial branch of KVIV. Among the vibration characteristics of a VIV oscillator in the initial branch is its quasi-periodic nature (Khalak and Williamson, 1999), which implies a modulated vibration amplitude along the time axis, where it increases and decreases cyclically. This is most simply demonstrated through a full flow time visualisation of y^* at $U^* = 4.5$, shown in Fig. 1, which bears striking resemblance to Fig. 15 of (Khalak and Williamson, 1999).
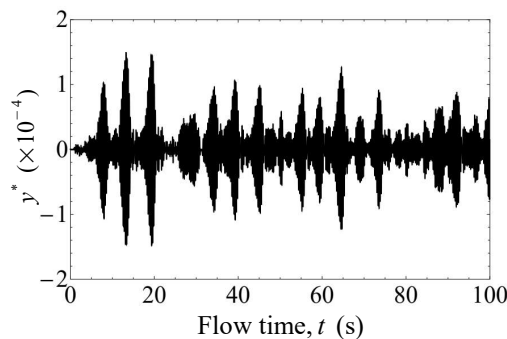

Figure 1: Full flow time visualisation of y^* at $U^* = 4.5$

Our choice of omitting the full flow time in our Hilbert-Huang transform (HHT) analysis is because the pre-processing algorithm EEMD is computationally expensive (Lv, 2019; Shifat and Hur, 2020), and we therefore limit ourselves only to a subset of the data instead.

Comment R2.8

How it's possible that $P_{Fluid,RMS} < P_{Mech.,RMS}$ for a given reduced velocity (Fig 20)?

Answer to R2.8

Unlike the original equation to compute fluid power, shown in Eq. 3,

$$P_{\text{Fluid,RMS}} = \frac{1}{2}\rho\pi C_{\text{Cl,RMS}}U^2 f_{\text{cyl.}} y^*_{\text{RMS}} DL \sin(\phi), \tag{3}$$

the original form of the equation in Raghavan (2007) used what basically amounts to maximum lift amplitude C_y in place of $C_{\text{Cl,RMS}}$, and the maximum cylinder displacement amplitude $y_{\text{max.}}$ in place of y^*_{RMS}.

As mentioned in the original manuscript,

> " We use C_{Cl,y^*} to represent $C_{\text{Cl,RMS}}$ in Eq. 26. We choose to use root-mean-square (parameters with subscript RMS) quantities in Eq. 25 instead of the maximum values like the original authors because that may lead to a misunderstanding that the maximum value is sustained throughout the observation window. "

Therefore, $P_{\text{Fluid,RMS}}$ as defined in Eq. 3 estimates the root-mean-square power obtainable from the streamwise component of lift alone, and not the total lift acting on the cylinder. This means that $P_{\text{Fluid,RMS}}$ will only be approximately equal to $P_{\text{Mech.,RMS}}$ if $C_{\text{Cl,RMS}}$ is the dominant component of the total lift **and** the phase lag ϕ is close to 90°. The observation $P_{\text{Fluid,RMS}} < P_{\text{Mech.,RMS}}$ made by the reviewer simply means that these conditions are not satisfied.

Comment R2.9

The fluid power is possible to improve by redirect the energy from the Karman to the streamwise vortex, and how it realizes? It's suggested to clarify a possible measure for it, or try to put forward an example.

Answer to R2.9

In the SVIV regime, the energy carried by the freestream is converted into three components, namely,

1. the generation of turbulence,

2. the production of streamwise vortices, and

3. the generation of Karman vortices.

In other words,

$$\text{Freestream energy} = \text{Turbulence} + \text{Streamwise vortices} + \text{Karman vortices}. \tag{4}$$

To improve the power output of a cruciform energy harvester in the SVIV regime, the basic idea is to maximise the conversion of freestream energy into streamwise vortices, amplifying the root-mean-square amplitude of the streamwise component of lift. One possible method to achieve this is by modifying the strip plate, which essentially is a passive downstream control mechanism, in a manner that enforces the dominance of the vortical structure that is able to lock into the natural frequency of the system f_n. This will lead to a larger C_{Cl,y^*}, C_{y^*,y^*}, ultimately $P_{\text{Fluid,RMS}}$ and $P_{\text{Mech.,RMS}}$. This is the subject of our next publication. However, following the suggestion of the reviewer, we deleted the following sentence,

" We shall detail in our future work, a method to modulate the dominant vortical structures to achieve such a goal. "

and included the following sentences in its place.

One possible method of improving $P_{\text{Fluid,RMS}}$ is by implementing a modified version of the cruciform that is able to enforce the dominance of the vortical structure that is able to lock into f_n - which in Fig. 22 is the streamwise vortex - against the vortical structures that do not, i.e., the Karman vortices. We will outline such a method in our future work.

References

Deng, J., Ren, A.L., Shao, X.M., 2007. The flow between a stationary cylinder and a downstream elastic cylinder in cruciform arrangement. Journal of Fluids and Structures 23, 715–731. URL: https://www.sciencedirect.com/science/article/pii/S0889974606001472, doi:10.1016/J.JFLUIDSTRUCTS.2006.11.005.

Ding, L., Bernitsas, M.M., Kim, E.S., 2013. 2-D URANS vs. experiments of flow induced motions of two circular cylinders in tandem with passive turbulence control for 30,000. Ocean Engineering 72, 429–440. URL: http://www.sciencedirect.com/science/article/pii/S0029801813002448?via%3Dihub, doi:10.1016/J.OCEANENG.2013.06.005.

Ding, W., Sun, H., Xu, W., Bernitsas, M.M., 2019. Numerical investigation on interactive FIO of two-tandem cylinders for hydrokinetic energy harnessing. Ocean Engineering 187, 106215. URL: https://www.sciencedirect.com/science/article/pii/S0029801819304019, doi:10.1016/J.OCEANENG.2019.106215.

Hemsuwan, W., Sakamoto, K., Nakada, S., Takahashi, T., 2018a. A longitudinal vortex wind turbine: Numerical study. Journal of Wind Engineering and Industrial Aerodynamics 180, 213–230. URL: https://www.sciencedirect.com/science/article/pii/S0167610518301612, doi:10.1016/J.JWEIA.2018.07.022.

Hemsuwan, W., Sakamoto, K., Nakada, S., Takahashi, T., 2018b. A longitudinal vortex wind turbine: Numerical study. Journal of Wind Engineering and Industrial Aerodynamics 180, 213–230. URL: https://www.sciencedirect.com/science/article/pii/S0167610518301612, doi:10.1016/J.JWEIA.2018.07.022.

Hemsuwan, W., Sakamoto, K., Takahashi, T., 2018c. Numerical investigation of lift-force generation on a moving circular cylinder in a uniform flow driven by longitudinal vortex. Journal of Fluids and Structures 83, 448–470. URL: https://www.sciencedirect.com/science/article/pii/S0889974617308885, doi:10.1016/J.JFLUIDSTRUCTS.2018.09.010.

Kato, N., Koide, M., Takahashi, T., Shirakashi, M., 2006. Influence of Cross-Sectional Configuration on the Longitudinal Vortex Excitation of the Upstream Cylinder in Cruciform Two-Cylinder System. Journal of Fluid Science and Technology 1, 126–137. URL: http://joi.jlc.jst.go.jp/JST.JSTAGE/jfst/1.126?from=CrossRef, doi:10.1299/jfst.1.126.

Kato, N., Koide, M., Takahashi, T., Shirakashi, M., 2012. VIVs of a circular cylinder with a downstream strip-plate in cruciform arrangement. Journal of Fluids and Structures 30, 97–114.

Khalak, A., Williamson, C., 1999. Motions, Forces And Mode Transitions In Vortex-Induced Vibrations At Low Mass-Damping. Journal of Fluids and Structures 13, 813–851. URL: http://www.sciencedirect.com/science/article/pii/S0889974699902360, doi:10.1006/jfls.1999.0236.

Koide, M., Ootani, K., Yamada, S., Takahashi, T., Shirakashi, M., 2006. Vortex Excitation Caused by Longitudinal Vortices Shedding from Cruciform Cylinder System in Water Flow. JSME International Journal 49, 1043–1048.

Koide, M., Sekizaki, T., Yamada, S., Takahashi, T., Shirakashi, M., 2013. Prospect of Micro Power Generation Utilizing VIV in Small Stream Based on Verification Experiments of Power Generation in Water Tunnel. Journal of Fluid Science and Technology 8, 294–308. doi:10.1299/jfst.8.294.

Koide, M., Takahashi, T., Shirakashi, M., Salim, S.A.Z.B.S., 2017. Three-dimensional structure of longitudinal vortices shedding from cruciform two-cylinder systems with different geometries. Journal of Visualization , 1–11.

Lv, H., 2019. Noise suppression of microseismic data based on a fast singular value decomposition algorithm. Journal of Applied Geophysics 170, 103831. doi:10.1016/j.jappgeo.2019.103831.

Nguyen, T., Koide, M., Takahashi, T., Shirakashi, M., 2010. Universality of longitudinal vortices shedding from a cruciform two circular cylinder system in uniform flow. Journal of Fluid Science and Technology 5, 603–616.

Nguyen, T., Koide, M., Yamada, S., Takahashi, T., Shirakashi, M., 2012. Influence of mass and damping ratios on VIVs of a cylinder with a downstream counterpart in cruciform arrangement. Journal of Fluids and Structures 28, 40–55. doi:10.1016/j.jfluidstructs.2011.10.006.

Raghavan, K., 2007. Energy Extraction from a Steady Flow Using Vortex Induced Vibration. Doctoral dissertation. The University of Michigan. URL: http://deepblue.lib.umich.edu/handle/2027.42/55687.

Shifat, T.A., Hur, J.W., 2020. EEMD assisted supervised learning for the fault diagnosis of BLDC motor using vibration signal. Journal of Mechanical Science and Technology 34, 3981–3990. URL: https://link.springer.com/article/10.1007/s12206-020-2208-7, doi:10.1007/s12206-020-2208-7.

Shirakashi, M., Mizuguchi, K., Bae, H.M., 1989. Flow-induced excitation of an elastically-supported cylinder caused by another located downstream in cruciform arrangement. Journal of Fluids and Structures 3, 595–607. doi:10.1016/S0889-9746(89)90150-3.

Shirakashi, M., Takahashi, T., Kumagai, I., Matsumoto, T., 2001. Vortex-induced vibration of the upstream cylinder of a two-cylinder system in cruciform arrangement. JCAM 2, 103–122.

Wang, J., Zhao, W., Su, Z., Zhang, G., Li, P., Yurchenko, D., 2020. Enhancing vortex-induced vibrations of a cylinder with rod attachments for hydrokinetic power generation. Mechanical Systems and Signal Processing 145, 106912. doi:10.1016/j.ymssp.2020.106912.

Zhao, M., Lu, L., 2018. Numerical simulation of flow past two circular cylinders in cruciform arrangement. Journal of Fluid Mechanics 848, 1013–1039. URL: `https://www.cambridge.org/core/product/identifier/S0022112018003804/type/journal_article`, doi:10.1017/jfm.2018.380.